# The Potential of Landsat 8 OLI Images in Coastline Identification: The Case Study of Basra, Iraq

**Hamzah Tahir**
Geoinformation Department, Faculty of Built Environment and Surveying, University Technology Malaysia, Malaysia
hamzahtahir1991@gmail.com (corresponding author)

**Ami Hassan Md. Din**
Geoinformation Department, Faculty of Built Environment and Surveying, University Technology Malaysia, Malaysia
amihassan@utm.my

*Received: 1 November 2023 | Revised: 3 December 2023 | Accepted: 6 December 2023*

 *DOI: https://doi.org/10.48084/etasr.6580*

**ABSTRACT**

**Coastline extraction plays important functions in coastal resource management, natural resource preservation, and sustainable coastal development. Long-term records of Landsat data series are available for free downloading, being highly potential for coastline extraction. Furthermore, remote sensing imagery systems along with the application of digital image processing techniques can be utilized in coastline extraction. However, it is challenging to accurately extract coastlines with coarse spatial resolution due to the dynamic properties of various types of coastlines produced by sea-level changes from tides and storms. Moreover, the use of conventional surveys and the need for high-resolution images involve substantial costs and efforts, especially when coastlines of long distances are involved. The current study compared the accuracy of extracting coastlines from Landsat 8 OLI with the observed coastlines from GPS data. In particular, this study focused on distinguishing water areas from non-water areas on the coastline of a selected concrete port. The analysis involved the use of both MNDWI and NDWI indexes. The statistical results demonstrated the accuracy of MNDWI (RMSE of 2.363) and NDWI (RMSE of 2.491 m), which suggested the potential of using Landsat 8 OLI in coastline identification.**

***Keywords-coastline extraction; Landsat 8 OLI; remote sensing***

## I. INTRODUCTION

Unlike most ocean-sensing equipment, the Landsat 8 satellite displays higher spatial resolution and sensitivity to color and illumination, providing highly accurate images. More importantly, the images can be generated at wavelengths that allow the identification of deformation caused by the atmosphere, especially when coastal areas are involved. Landsat 8 consists of two sensors, namely an Operational Land Imager (OLI) and a Thermal Infrared Sensor (TIRS). The data gathered are readily available for free download via GloVis, Earth Explorer, and Landsat Look Viewer [1].

Coastal areas are subjected to threats caused by human activities and natural phenomena, such as coastal erosion-accretion and sea-level changes. Authors in [2-4] argued the importance of representing the coastline and identifying adverse human activities for the sustainability of coastal communities. Despite the beneficial use of conventional ground surveys in creating coastline maps [4], the incorporation of grounding survey data and images into coastal maps takes up too much time and can be rather costly [4, 5]. Meanwhile, remote sensing is often used to map coastlines and detect related changes due to its macroscopic, real-time, dynamic, and cost-effective features, as well as its broad range of spatial and temporal scales [4, 6, 7]. For instance, authors in [8, 9] utilized the simulated degraded Landsat images in a smooth classification approach for the collection of sub-pixel-scale shorelines, with a Root Mean Square Error (RMSE) of 2.25 m. Authors in [10] suggested the utilization of Landsat TM and ETM+ for the extraction of sub-pixel-scale shorelines, with RMSE ranging from 4.69 m to 5.47 m. Authors in [11] utilized Landsat MSS and TM MS images to monitor the Chinese coastline, which revealed a statistically significant Mean Net Shoreline Movement (MNSM) of 2.54 m and a Mean Absolute Difference (MAD) of 11.26 m. Meanwhile, authors in [12, 13] utilized Landsat images to observe the annual mean shoreline positions with the goal of reducing the short-term variability of shorelines. The study observed that the

retrieved shorelines were biased seaward by 4 m to 5 m, which was attributed to the shift of the natural beaches over time.

The current study focuses on the effective statistical evaluation of determining the error in coastline extraction through the use of Landsat 8 OLI, which would help researchers and practitioners in data construction and analysis.

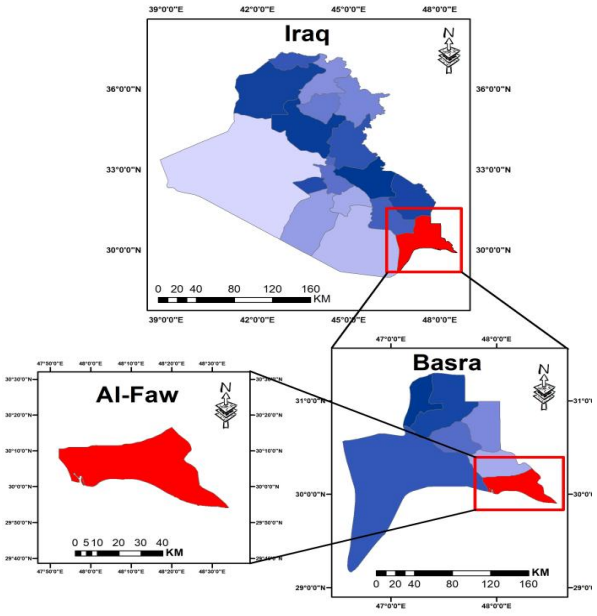


Fig. 1. Case study.

## II. STUDY AREA AND DATA

### A. Study Area

In this study, data from Landsat 8 OLI were collected on 12 December 2022. The retrieved data represented Basra City in southern Iraq, which officially divides Kuwait and Iran. Basra is the only Iraqi harbour with a view of the Gulf, which stretches for approximately 60 km. Its strategic location and booming oil industry establish the city as a prime destination for international businesses. In addition, the majority of the residents in Basra reside in areas with easy access to water [14]. The recent economic growth of the city has contributed to substantial interest in topographic data, which are particularly crucial for future building projects that require more precise elevation. However, there are limited topographic data for Basra city, which are mainly confined to a few locations within the city. Referring to Figure 1, it is evident that little is known about the topography of the city center and its surrounding neighborhoods, such as Faro, Quran, and Abu Al-Khasab.

### B. Landsat 8 OLI

Landsat data series are typically considered when it comes to coastline extraction due to their ease-of-access feature and extensive history of data collection and revisit coverage. As for the current study, one Landsat 8 OLI multispectral (MS) image, which covers an area of 185×180 km along the track, and one PAN image, which covers the same area for coastline extraction, were acquired. As of 29 December 2022 at 16:03 (UTC), the original Landsat 8 OLI image from path 165 and row 039 was downloaded as a land surface reflectance product in GeoTIFF format from Earth Explore (http://earthexplorer.usgs.gov/). Landsat 8 OLI images were acquired from the World Geodetic System (WGS84) data. Meanwhile, the final product involved the use of UTM projection. The details of OLI images from Landsat 8 are summarized in Table I.

TABLE I. PROPERTIES AND APPLICATIONS OF LANDSAT 8 BANDS [11]

| Landsat 8 Sensors | Band | Wavelength (μm) | Name of the Band | Resolution (m) |
|---|---|---|---|---|
| OLI | 1 | 0.433 – 0.453 | Coastal/Aerosol | 30 |
| | 2 | 0.450 – 0.515 | Blue | |
| | 3 | 0.525 – 0.600 | Green | |
| | 4 | 0.630 – 0.680 | Red | |
| | 5 | 0.845 – 0.885 | Near-infrared (NIR) | |
| | 6 | 1.560 – 1.660 | Short-wave infrared (SWIR) 1 | |
| | 7 | 2.100 – 2.300 | SWIR 2 | |
| | 8 | 0.500 – 0.680 | Panchromatic | 15 |
| | 9 | 1.360 – 1.390 | Cirrus | 30 |
| TIRS | 10 | 10.30 – 11.30 | Long-wave infrared (LWIR) 1 | 100* |
| | 11 | 11.50 – 12.50 | LWIR 2 | |
| | BQA | | Quality Assessment | |

*TIRS bands were originally acquired at a resolution of 100 m, but this was reduced to 30 m in the final data product.

### C. GPS Data

When it comes to the Global Positioning System (GPS), numerous observation methods are available for use. As for the current study, the rapid static relative positioning and Real-Time Kinematic (RTK) methods were selected to observe all points due to their accuracy and the shorter time required for observation [15, 16]. Rapid static relative positioning and kinematic survey methods are distinctly different in terms of duration. The results from one epoch can potentially be used to determine the location of a roving receiver in a kinematic survey. An epoch rate of 1 s is typically employed for a kinematic survey. The accuracy of intermediate points is within the range of ±1–2 cm + 2 ppm. The rapid static relative positioning method records ± 3–5 mm + 1 ppm and requires 10 min + 1 min/km, whereas the RTK method has the capacity to establish rover positions at intervals of as short as 0.2 s. On the other hand, establishing reference points in a static survey requires a substantially longer time. In most cases, the accuracy of a kinematic survey is dissimilar from that of a static survey [17]. In this study, the rapid static survey method was used to establish the reference point, and the coastline reference points were observed using the RTK method. As shown in Figure 2, the Ground Control Points (GCPs) were subjected to observation.

## III. METHODOLOGY

### A. Data Preparation

In this study, the reference distance values were compared with Landsat 8 OLI images created within the context of GIS (coastline values from Landsat 8 OLI in correspondence to the coastline from GCPs). ArcGIS 10.1 was used for this study's

data conversion and preparation. The same horizontal data were used for both data sets in this study. The reference data of the research site were converted into the same projection system—zone 38 north of the Universal Transverse Mercator (UTM). In particular, WGS1984 represented this study's geodetic and spheroid.

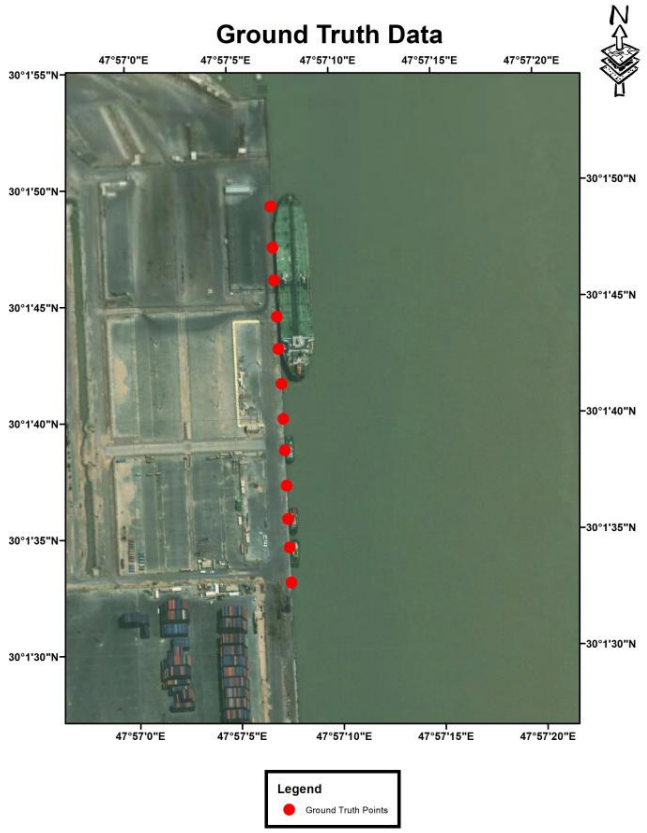


Fig. 2. Coastline reference of GPS using the RTK method.

## B. Pan-sharpening Algorithms

Numerous algorithms have been developed with the objective of creating a perfect spatial resolution MS image through the combination of PAN and MS bands. The process involved is known as pan-sharpening [18]. As a data fusion technique, pan-sharpening involves the high spatial resolution of a PAN image and the coarse spatial resolution of an MS image to construct a sharpened MS image with the same spatial resolution as the PAN image. Pan-sharpening enhances spatial resolution and retains the spectral characteristic of the primary MS image [19, 20]. The combination of Landsat ETM and MS and PAN bands typically involves this process of pan-sharpening for improved land use or cover mapping, precision farming, environment monitoring, forest management inventory, and urban areas scoping [20-24]. Accordingly, there are 7 MS bands with a spatial resolution of 30 m and a PAN band with a spatial resolution of 15 m in the recently released Landsat 8 OLI images [25]. With that, the use of pan-sharpening on Landsat 8 30 m MS image and the 15 m PAN band generates a 15 m spatial resolution-fused MS image.

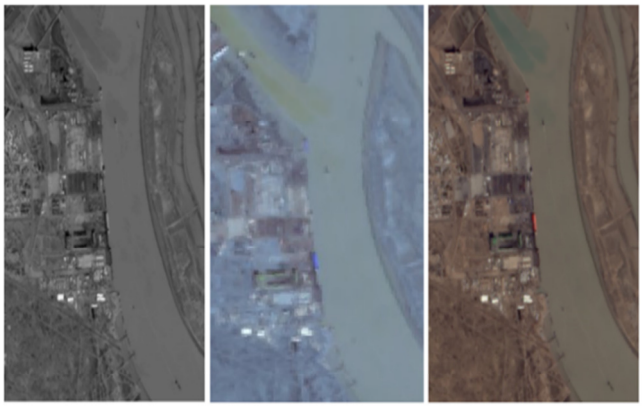


Fig. 3. The proposed pan-sharpening method for Study using GIS.

## C. Water Indexes

### 1) Normalized Difference Water Index (NDWI)

NDWI [26] is frequently used to detect remotely sensed coastlines. This index highlights the presence of water in a remotely sensed image using the green band and NIR band [26, 27].

$$NDWI = \frac{\rho Green - \rho NIR}{\rho Green + \rho NIR} \quad (1)$$

where $\rho Green$ is the reflectance value of the green band in the MS image and $\rho NIR$ is the reflectance value of the NIR band in the MS image.

This index uses green wavelengths to enhance water reflectance, reduce NIR reflectance by water features, and maximize NIR reflectance by vegetation and soil features. Hence, water characteristics are accentuated, while vegetation and soil are repressed. The calculated index ranges between 0 and 1. A negative value indicates a non-water surface, while a positive value indicates a water surface. An MS image with one green band and one NIR band can be used to determine the NDWI [26].

### 2) Modified Normalized Difference Water Index (MNDWI)

MNDWI deals with the limitations of NDWI that often fail to distinguish water-related information from built-up land noise, resulting in the overemphasis of the extracted water areas. Apart from enhancing open water features, the use of MNDWI can effectively suppress and eliminate built-up land noise, vegetation noise, and soil noise. The strengths of MNDWI in reducing and eliminating built-up land noise make it a preferred choice when it comes to the need to augment and extract water-related information for a water area with its background dominated by built-up land areas [28]. The index is expressed as:

$$MNDWI = \frac{\rho Green - \rho MIR}{\rho Green + \rho MIR} \quad (2)$$

where $\rho Green$ is the reflectance value of the green band in the MS image and $\rho MIR$ is the Middle-Infrared Band.

In comparison to NDWI, MNDWI yields a significantly wider contrast between water and built-up land due to the increase of water feature values and the decrease of built-up land values (from positive to negative). Greater enhancement of water in the MNDWI image results in higher accuracy in the extraction of open water features considering the negative values of built-up land, soil, and vegetation.

### *D. Statistical Analysis*

The assessment of Landsat 8 OLI in this study involved a statistical approach. Statistical analysis can enhance the interpretation of Landsat 8 OLI and GPS dataset correlations, trends, and error propagation. The difference in values between the coastline model of Landsat 8 OLI and the coastline reference of GPS would generate the distance error for each point:

$$D_{Diff} = D_{Model} - D_{Reference} \quad (3)$$

where $D_{Diff}$ is the distance difference, $D_{Model}$ is the coastline model of Landsat 8 OLI and $D_{Reference}$ is the coastline reference of GPS.

Mean Error (ME), Standard Deviation (STD), and RMSE, which are commonly used to evaluate the precision of continuous variables, were computed for each model.

$$ME = \sum_{i-1}^{n} \frac{D_{diff}}{N} \quad (4)$$

$$STD = \sqrt{\frac{(D_{diff} - ME)^2}{N-1}} \quad (5)$$

$$RMSE = \sqrt{\sum_{i-1}^{n} \frac{(D_{diff}{}^2)}{N}} \quad (6)$$

Accordingly, RMSE is associated with the assessment of surface quality and indicates the differences between variables (predicted by the model and observed data), where *N* denotes the total element number [29]. The reference distance values were compared with Landsat 8 data.

## IV. RESULTS AND DISCUSSION

The current study primarily focused on determining the distance error values in terms of STD and RMSE for each point between the coastline of Landsat 8 OLI and the reference coastline of GPS. MS Excel and GIS were used. This study gathered Landsat 8 OLI from the USGS website. All distances were measured using GIS. Methods to extract coastline from Landsat 8 OLI bands were developed. MS band (Red, Green, and Blue), NIR band, and Panchromatic (PAN) band of Landsat 8 OLI image were primarily used in this study. The green band and NIR band were used to calculate NDWI from (1). Through the combination of Landsat 8 OLI and MS and PAN bands, the use of pan-sharpening algorithm produced a 15 m sharpened MS image. Following that, the original Landsat 8 OLI-MS bands were utilized to calculate MNDWI images with (2). Finally, the conversion of water/non-water images into the vector format was performed using ArcGIS to extract the coastline (Figure 4). Table II summarizes the obtained statistical results.

TABLE II. STATISTICAL RESULTS OF THE VALIDATION OF DISTANCE VALUES FOR LANDSAT 8 OLI IMAGE

| Index | Min. | Max. | Mean | STD | RMSE | Min. |
|---|---|---|---|---|---|---|
| **MNDWI** | 0.62 | 3.153 | 2.156 | 2.466 | 2.363 | 0.62 |
| **NDWI** | 0.622 | 3.167 | 2.304 | 2.606 | 2.491 | 0.622 |

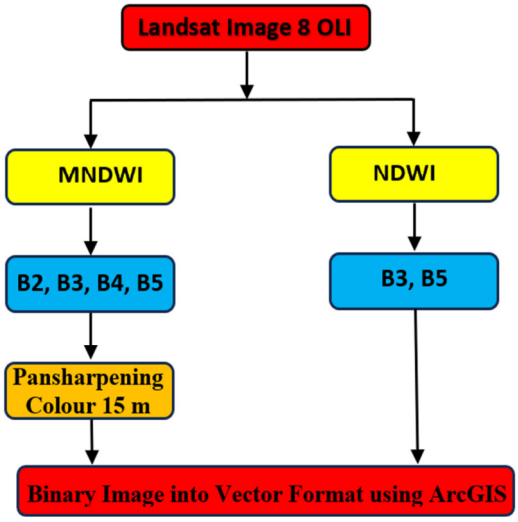


Fig. 4. Strategy used to calculate the coastline from the Landsat 8 OLI image.

In particular, the MNDWI index recorded higher accuracy (STD = 2.466, RMSE = 2.363) than the NDWI (STD = 2.606, RMSE = 2.491). The use of pan-sharpening algorithm in this study generated sharpened MS images in standard false color at a spatial resolution of 15 m. As previously shown in Figure 3, the original 30 m MS image and 15 m PAN image were subjected to statistical analysis. The MS RBG bands 2, 3, and 4 in the Landsat 8 OLI image were used for this purpose.

The generated fused MS images were then used for the generation of the corresponding NDWI and MDWI images, which are provided in Figure 6. Critical spectral distortion of bands 3 and 5 was observed for the case of pan-sharpening algorithms. As a result, this study found indistinguishable water and non-water features in the calculated NDWI images, as depicted in Figure 6(b) (within the red circles).

## V. CONCLUSION

The novelty of this study is that it employs highly accurate GPS data to provide a precise evaluation of the coastline that has been previously extracted by researchers [11, 28]. Statistical analysis focused on the distance values for each index in terms of STD and RMSE between GPS and Landsat 8 OLI images. Minimum value, maximum value, and ME were considered. The distance between the coastline of Landsat 8 OLI and the reference coastline of GPS was first calculated. Statistically, MDWI (RMSE of 2.363 m) recorded higher accuracy than NDWI (RMSE = 2.491). Based on the obtained results, this study presented an accurate statistical evaluation of determining the error in coastline extraction through the use of Landsat 8 OLI images, which would benefit researchers and practitioners in data construction and analysis. Moreover, this study demonstrated the promising potential of using Landsat 8

OLI in coastline identification. The cost- and time-effectiveness of Landsat 8 OLI make it a crucial tool when it comes to inundation maps and other applications.

(a)

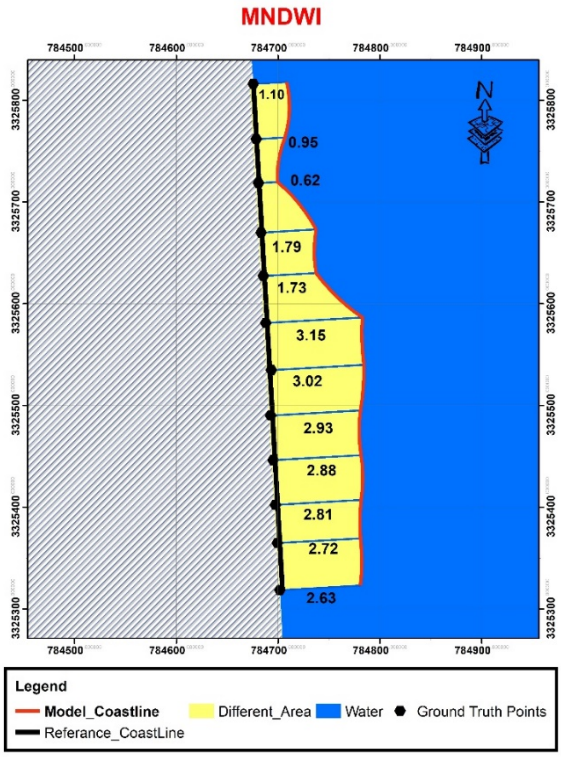


(b)

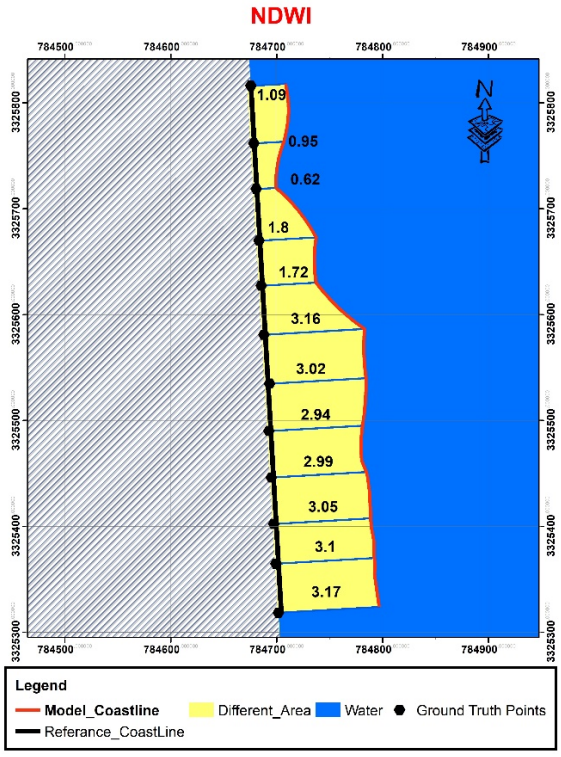


Fig. 5. Distance difference between the coastline reference of GPS and the coastline of Landsat 8 OLI by (a) MNDWI and (b) NDWI.

(a)

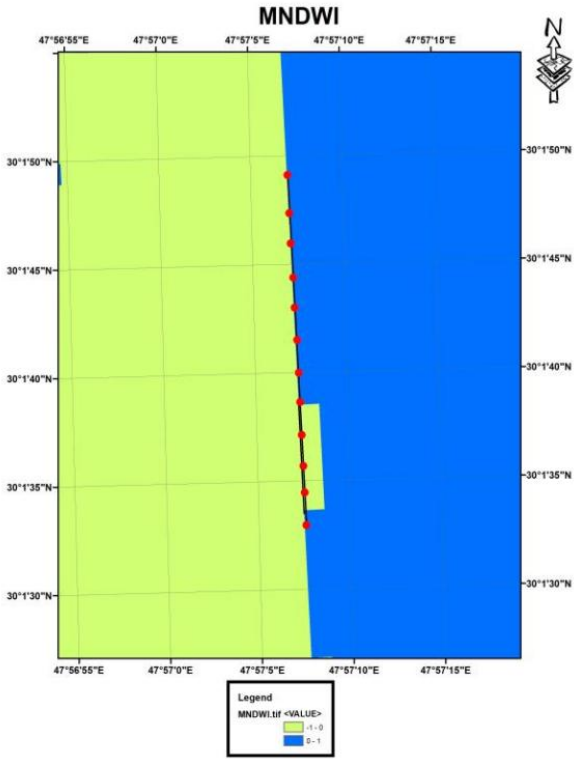


(b)

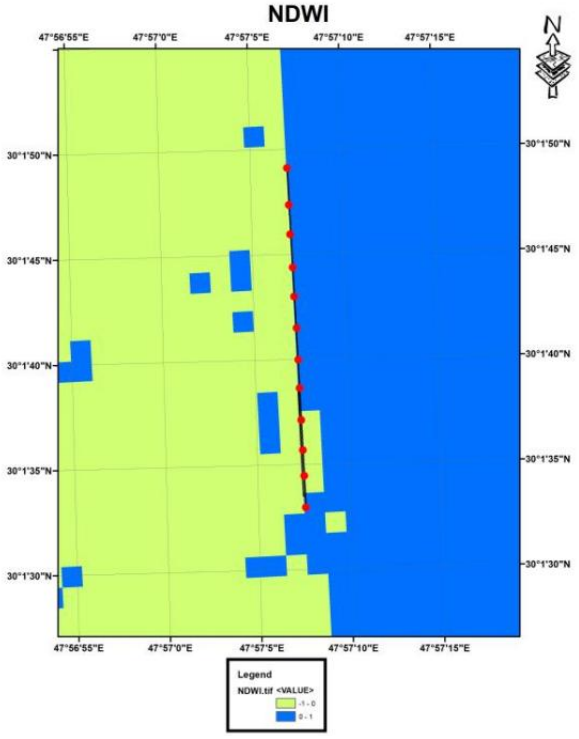


Fig. 6. Water and non-water feature maps by (a) MNDWI and (b) NDWI using GIS.

## AUTHOR CONTRIBUTION

H. Tahir and A. H. M. Din jointly planned and designed the study. H. Tahir analyzed the data and authored the first draft of

the manuscript, whereas A. H. M. Din provided essential data and facilities and significantly contributed to discussion, data analysis, and test preparation.

## REFERENCES

[1] T. Acharya and I. Yang, "Exploring Landsat 8," *International Journal of IT, Engineering and Applied Sciences Research*, vol. 4, no. 4, pp. 4–10, May 2015.

[2] L. J. Moore, "Shoreline Mapping Techniques," *Journal of Coastal Research*, vol. 16, no. 1, pp. 111–124, 2000.

[3] M. K. Villareal and A. F. Tongco, "Remote Sensing Techniques for Classification and Mapping of Sugarcane Growth," *Engineering, Technology & Applied Science Research*, vol. 10, no. 4, pp. 6041–6046, Aug. 2020, https://doi.org/10.48084/etasr.3694.

[4] R. Aedla, G. S. Dwarakish, and D. V. Reddy, "Automatic Shoreline Detection and Change Detection Analysis of Netravati-GurpurRivermouth Using Histogram Equalization and Adaptive Thresholding Techniques," *Aquatic Procedia*, vol. 4, pp. 563–570, Jan. 2015, https://doi.org/10.1016/j.aqpro.2015.02.073.

[5] R. S. Dewi, W. Bijker, A. Stein, and M. A. Marfai, "Fuzzy Classification for Shoreline Change Monitoring in a Part of the Northern Coastal Area of Java, Indonesia," *Remote Sensing*, vol. 8, no. 3, Mar. 2016, Art. no. 190, https://doi.org/10.3390/rs8030190.

[6] W. Li and P. Gong, "Continuous monitoring of coastline dynamics in western Florida with a 30-year time series of Landsat imagery," *Remote Sensing of Environment*, vol. 179, pp. 196–209, Jun. 2016, https://doi.org/10.1016/j.rse.2016.03.031.

[7] E. H. Boak and I. L. Turner, "Shoreline Definition and Detection: A Review," *Journal of Coastal Research*, vol. 21, no. 4, pp. 688–703, 2005.

[8] G. M. Foody, A. M. Muslim, and P. M. Atkinson, "Super-resolution mapping of the waterline from remotely sensed data," *International Journal of Remote Sensing*, vol. 26, no. 24, pp. 5381–5392, Dec. 2005, https://doi.org/10.1080/01431160500213292.

[9] M. V. Japitana and M. E. C. Burce, "A Satellite-based Remote Sensing Technique for Surface Water Quality Estimation," *Engineering, Technology & Applied Science Research*, vol. 9, no. 2, pp. 3965–3970, Apr. 2019, https://doi.org/10.48084/etasr.2664.

[10] J. E. Pardo-Pascual, J. Almonacid-Caballer, L. A. Ruiz, and J. Palomar-Vázquez, "Automatic extraction of shorelines from Landsat TM and ETM+ multi-temporal images with subpixel precision," *Remote Sensing of Environment*, vol. 123, pp. 1–11, Aug. 2012, https://doi.org/10.1016/j.rse.2012.02.024.

[11] Y. Liu, X. Wang, F. Ling, S. Xu, and C. Wang, "Analysis of Coastline Extraction from Landsat-8 OLI Imagery," *Water*, vol. 9, no. 11, Nov. 2017, Art. no. 816, https://doi.org/10.3390/w9110816.

[12] J. Almonacid-Caballer, E. Sánchez-García, J. E. Pardo-Pascual, A. A. Balaguer-Beser, and J. Palomar-Vázquez, "Evaluation of annual mean shoreline position deduced from Landsat imagery as a mid-term coastal evolution indicator," *Marine Geology*, vol. 372, pp. 79–88, Feb. 2016, https://doi.org/10.1016/j.margeo.2015.12.015.

[13] V. Kumar *et al.*, "GIS-Based Analysis of a Rainwater Harvesting System in the Multipurpose Hall of Quaid-e-Awam University of Engineering, Science, and Technology," *Engineering, Technology & Applied Science Research*, vol. 12, no. 4, pp. 8837–8842, Aug. 2022, https://doi.org/10.48084/etasr.4995.

[14] I. Al-abboodi, A. Hamoody, and S. Saleh, "Geotechnical Features of Basrah City, Iraq," *Basrah Journal for Engineering Sciences*, vol. 20, pp. 1–7, Mar. 2020, https://doi.org/10.33971/bjes.20.2.1.

[15] A. Mohammed *et al.*, "A Landscape of Research on Bus Driver Behavior: Taxonomy, Open Challenges, Motivations, Recommendations, Limitations, and Pathways Solution in Future," *IEEE Access*, vol. 9, pp. 139896–139927, 2021, https://doi.org/10.1109/ACCESS.2021.3102222.

[16] S. N. Abdulwahid, M. A. Mahmoud, H. M. Gheni, S. A. Mostafa, and A. Mohammed, "A Systematic Review on Motorcyclists' Aggressive Behavior Analysis Using Computational Models: Current State, Challenges, and Recommendations," *Journal of Theoretical and Applied Information Technology*, vol. 100, no. 16, pp. 5032–5055, Aug. 2022.

[17] C. Wolff *et al.*, "A Mediterranean coastal database for assessing the impacts of sea-level rise and associated hazards," *Scientific Data*, vol. 5, no. 1, Mar. 2018, Art. no. 180044, https://doi.org/10.1038/sdata.2018.44.

[18] B. Aiazzi, S. Baronti, and M. Selva, "Improving Component Substitution Pansharpening Through Multivariate Regression of MS +Pan Data," *IEEE Transactions on Geoscience and Remote Sensing*, vol. 45, no. 10, pp. 3230–3239, Jul. 2007, https://doi.org/10.1109/TGRS.2007.901007.

[19] I. Amro, J. Mateos, M. Vega, R. Molina, and A. K. Katsaggelos, "A survey of classical methods and new trends in pansharpening of multispectral images," *EURASIP Journal on Advances in Signal Processing*, vol. 2011, no. 1, Sep. 2011, Art. no. 79, https://doi.org/10.1186/1687-6180-2011-79.

[20] Q. Xu, Y. Zhang, and B. Li, "Recent advances in pansharpening and key problems in applications," *International Journal of Image and Data Fusion*, vol. 5, no. 3, pp. 175–195, Jul. 2014, https://doi.org/10.1080/19479832.2014.889227.

[21] K. K. Lwin and Y. Murayama, "Evaluation of land cover classification based on multispectral versus pansharpened landsat ETM+ imagery," *GIScience & Remote Sensing*, vol. 50, no. 4, pp. 458–472, Aug. 2013, https://doi.org/10.1080/15481603.2013.814279.

[22] T. Wang *et al.*, "Geometric Accuracy Validation for ZY-3 Satellite Imagery," *IEEE Geoscience and Remote Sensing Letters*, vol. 11, no. 6, pp. 1168–1171, Jun. 2014, https://doi.org/10.1109/LGRS.2013.2288918.

[23] A. Mohammed and M. R. M. Yazid, "Differences of Malaysian Bus Drivers Behaviours in Speeding, Acceleration and Deceleration Under Various Driving Conditions," *International Journal of Mechanical Engineering*, vol. 7, no. 1, pp. 1812–1820, 2022.

[24] A. H. Alamoodi *et al.*, "A systematic review into the assessment of medical apps: motivations, challenges, recommendations and methodological aspect," *Health and Technology*, vol. 10, no. 5, pp. 1045–1061, Sep. 2020, https://doi.org/10.1007/s12553-020-00451-4.

[25] J. Jong-Song and C. Jong-Hun, "Application Effect Analysis of Image Fusion Methods for Extraction of Shoreline in Coastal Zone Using Landsat ETM+," *International Journal of Atmospheric and Oceanic Sciences*, vol. 1, no. 1, pp. 1–6, Dec. 2017, https://doi.org/10.11648/j.ijaos.20170101.11.

[26] S. K. McFeeters, "The use of the Normalized Difference Water Index (NDWI) in the delineation of open water features," *International Journal of Remote Sensing*, vol. 17, no. 7, pp. 1425–1432, May 1996, https://doi.org/10.1080/01431169608948714.

[27] M. A. M. Alghamdi and A. Z. E. A. Bishta, "Preliminary Site Investigation based on RGB Electromagnetic Energy of Landsat-7 Images in Wadi Fayidah, Saudi Arabia," *Engineering, Technology & Applied Science Research*, vol. 13, no. 2, pp. 10595–10600, Apr. 2023, https://doi.org/10.48084/etasr.5800.

[28] H. Xu, "Modification of normalised difference water index (NDWI) to enhance open water features in remotely sensed imagery," *International Journal of Remote Sensing*, vol. 27, no. 14, pp. 3025–3033, Jul. 2006, https://doi.org/10.1080/01431160600589179.

[29] D. Athmania and H. Achour, "External Validation of the ASTER GDEM2, GMTED2010 and CGIAR-CSI- SRTM v4.1 Free Access Digital Elevation Models (DEMs) in Tunisia and Algeria," *Remote Sensing*, vol. 6, no. 5, pp. 4600–4620, May 2014, https://doi.org/10.3390/rs6054600.